 doi:10.20944/preprints202303.0394.v1

Article

Isoprene Emission under Climate Change Scenario in Southeast Asia

Franky Herman [1], Justin Sentian [1,*], Vivian Kong Wan Yee [1], Maggie Ooi Chel Gee[2] and Mohd Sharul Mohd Nadzir[3]

[1] Faculty of Science and Natural Resource, University Malaysia Sabah, UMS ROAD 88400 Kota Kinabalu, Malaysia; frankyhermn@gmail.com
[2] Insitute of Climate Change, Universiti Kebangsaan Malaysia, 43600 Bangi, Selangor, Malaysia; chelgee.ooi@ukm.edu.my
[2] Department of Earth Sciences and Environment, Faculty of Sciences and Technology, Universiti Kebangsaan Malaysia, 43600, Bangi, Selangor, Malaysia; shahrulnadzir@ukm.edu.my
* Correspondence: jsentian@ums.edu.my

Abstract: Biogenic emission can have significant impact on atmospheric chemistry. Isoprene (C_5H_8) is known as the most predominant volatile organic compound and its emission is highly dependent on temperature and light (solar radiation). This study aims to investigate future changes of isoprene emission under climate change scenario. The Southeast Asia (SEA) region is home to 15% of the world's tropical forest, and the biogenic emission from this region can have significant effect on the global climate chemistry. Three climate change scenarios (RCP4.5, RCP6.0 and RCP8.5) were used to drive climate change simulation in 2013 (baseline), 2030 (near-future), 2050 (mid-century), 2070 (post-mid) and 2100 (end of century) using the Weather Research Forecasting (WRF v3.9.1) model. The Model Emission of Gases and Aerosol from Nature (MEGAN v2.1) was then used to simulate isoprene fluxes using climate output datasets from the WRF model. This study highlights that the projected mean surface temperature and PAR (photosynthetic active radiation) were higher in July than in January. Towards the end of the century, the overall surface temperature and PAR over the SEA region is expected to increase by 0.9°C - 2.1°C, and 7.6 W m^{-2} – 12 W m^{-2} under all RCPs. The all-time high isoprene emitters are Borneo and Papua Island. Meanwhile, the projected increment of isoprene emission over this region is between 10 – 14%, 15-30% and 29 – 53% for RCP4.5, RCP6.0 and RCP8.5, respectively. Our result concludes that the total isoprene emission was higher during July, consistent with the high surface temperature and PAR. The results also agreed with the hypothesis of high isoprene emission over the region that has oil palm plantation. Thus, challenges in dealing with future emissions of isoprene in SEA are closely tied to future climate policies to limit the warming of the atmosphere over this region and the land-use conversion of palm oil plantations.

Keywords: isoprene; climate change; SEA; WRF; MEGAN; temperature; PAR

1. Introduction

Biogenic volatile organic compounds (BVOCs) refer to all low boiling compounds which are stored in, synthesized, and emitted by secondary metabolic pathways in plants and vegetations. Volatile organic compounds (VOCs) emitted from plants and vegetations constitute the largest BVOC emission released into the atmosphere [1]. The primary source of BVOCs emission is the forest which contributes 70% of the total emission from vegetation. It was estimated that the total global annual BVOC emission was about 10^6 Gg C $year^{-1}$ [2]. At least 90% of the total annual emission are non-methane volatile organic compounds (NMVOC); therefore, the rest of the NMVOC was emitted from the anthropogenic source [3]. The NMVOCs species (such as benzene, xylene, propane, and butane) are important O_3 and SOA precursors, playing key roles in controlling the tropospheric chemistry budget [4]. The high concentration of O_3 particularly in the lower atmosphere

 doi:10.20944/preprints202303.0394.v1

is widely known to pose adverse impacts on human health [5], vegetation [6], and the surrounding built infrastructure [7].

Isoprene (C_5H_8) is the simplest carbon isoprenoid and represents the highest emission component from the total annual BVOCs emission followed by monoterpene ($C_{10}H_{16}$). It was estimated that the emission of both species can produce 400 – 600 Tg C year^{-1} for isoprene and 30 – 150 Tg C year^{-1} for monoterpene [2-3]. Furthermore, it was speculated that the emission tends to vary year by year due to climatic and environmental factors [8-10]. Both isoprene and monoterpene were synthesized and formed either constitutively or after stress induction was produced [11-12]. The emission is important in regulating the growth and reproduction of plants while improving the plants' tolerance against environmental stressors and preventing harm from animals and insects [13-14].

Much of BVOCs emission is controlled by environmental factors such as humidity [15-16], temperature [17-18], solar radiation [19]. These environmental factors act as physiological factors that influence the availability of plant substrate and limit the rate of enzyme activity within the plant stomata. The physiochemical constraints can enhance the synthase of the volatile molecules under the conditions at which isoprene emissions are highly optimum, i.e., at air temperature between 25-35°C, relative humidity between 50-60%, and photosynthetic photon flux between 800 and 1000 μmol m^{-2} s^{-1} [20-21]. Isoprene emission is expected to increase with global warming, particularly in the temperate and boreal regions [20]. Global warming will not just increase the overall surface air temperature, but also the atmospheric properties such as kinetic processes, chemistry reaction and rate, and the emission source of pollutants [22-23]. Therefore, warmer temperature will stimulate higher leaf emission promptly by enhancing cellular production rate and promoting higher LAI (leaf area index) [24-25], thus enhancing biogenic emission rate.

Improved understanding of BVOCs emission is important in the air chemistry and climate system. There is no observation of past BVOCs emission, and their pre-industrial baseline emission does not exist; thus, their estimations (and to extend their forcing) rely upon simulations based on pre-industrial conditions [25]. Further, the future changes in atmospheric BVOCs potentially counteract air pollutants and climate effects through anthropogenic emission controls [26]. Thus, the previous modelled present-day and future-day BVOCs studies have large uncertainties in the derived values, and more studies are required to further understand the emission characteristic and the relationship with air pollution and climate [27]. However, most studies on regional or global modelling in BVOC emission had only focused on dominant global sources, vegetation foliage, and other components that contribute to above-canopy fluxes [28].

Moreover, most isoprene emission rate measurement studies had focused on trees, and there is a relatively large database for assigning tree emission factors [29]. Vegetative emission has large inter-species variability, as well regional, temporal and seasonal variability [30]. Thus, the reported global values from diverse investigation methods used often differ from one another. Available literature and investigation on BVOCs in most Asian regions were generally limited because of the experimental and analytical difficulties [14]. Furthermore, most of the studies that investigated the climate change impact on biogenic emissions were largely focused on China [31-32] and the European region [33-34] while the recent study on SEA region only covered mainland SEA, such as Thailand [35] for only a specific period of time. Hence, the characteristics and behavior of the biogenic emission over the SEA region under changing climate conditions are not yet fully investigated.

2. Materials and Methods

2.1 Study Area

This study is limited to Southeast Asia, as it is a sub-region which lies between the tropics; therefore, there are similarities in climate as well as plant and animal life throughout the region. The climate condition in the SEA region can be categorized into two seasons namely the winter season during the northeast monsoon and the summer season

 doi:10.20944/preprints202303.0394.v1

during the southeast monsoon [36]. The climate is modulated by the Asian-Australian monsoon system [37] and the El~Niño-Southern Oscillation (ENSO) which has a critical factor in influencing the precipitation and temperature [38]. It is therefore important to model the emission of BVOC especially over the monsoon season so as to increase comprehensive understanding of the seasonal emission rate and the effect of changing climatic condition, hence enriching the existing research literature and method on atmospheric environment studies. Briefly, the relationship between BVOC emission and climate (especially temperature) is unclear in a prior study [39]. With the inclusion of climate change scenarios, this current study will highlight the relationship between future temperature and light / PAR (photosynthetic active radiation) with biogenic emiss

2.2. Model Setup and Configuration

2.2.1. WRF Model

This study used Weather Research Forecast version 3.9.1.1 (WRF V 3.9.1.1) as a regional climate modelling system. The domain, simulations and parameterization of the WRF model used under this study is similar to the study of [40]. The simulation was carried out in one nested horizontal domain (Figure 2.1). We used time-dependent meteorological fiend obtained from the global model of Operational Global Analysis at 0.25 degree by 0.25-degree grids (NCEP FNL) which is available at https://rda.ucar.edu/datasets/ds083.2. The NCEP FNL dataset consists of surface information with 26 mandatory levels (reaching from 1000 millibars to 10 millibars) of the surface boundary level. The meteorological parameters included temperature, sea surface temperature, sea level pressure, geopotential height, relative humidity, ice cover, vertical motion, vorticity, ozone, meridional, and zonal winds (NCEP, 2015). The surface layer scheme used for this study was the Revised MM5 Monin-Obukhov Scheme, while the Noah Land Surface Model (LSM) was used for land surface scheme, and the Thompson Aerosol-Aware Scheme for microphysics parameterization. Meanwhile, the Rapid Radiative Transfer Model (RRTM) and Dudhia Shortwave radiation were both used for longwave and shortwave radiation physics. To better simulate the climate over this region, we also used the Mellor-Yamada Janji Scheme as boundary layer for the WRF model setup and the Urban surface canopy model.

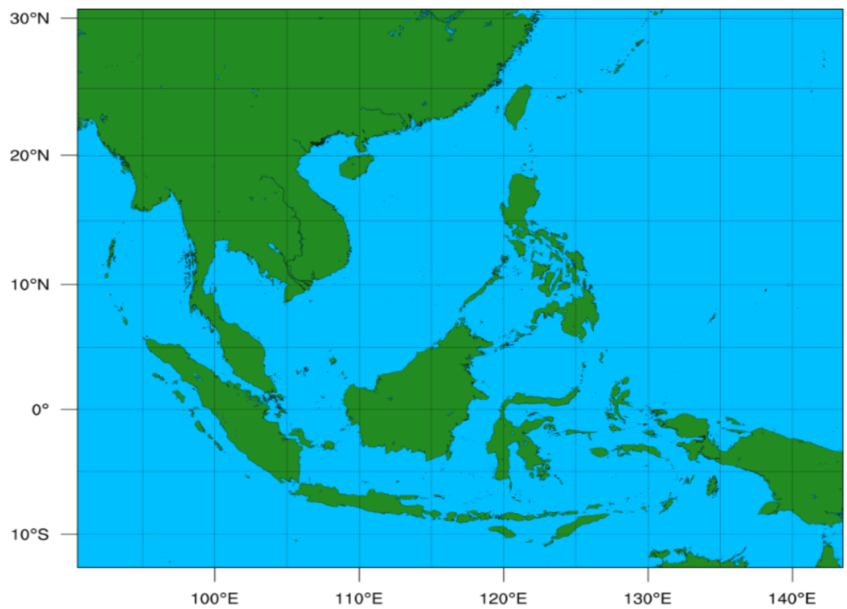

Figure 1. Research domain of Southeast Asia from the WRF model.

While for future day simulation, the NCAR's Community Earth System Model (CESM) from global bias-corrected climate model output files dataset was used as

Preprints (www.preprints.org) | NOT PEER-REVIEWED | Posted: 22 March 2023 doi:10.20944/preprints202303.0394.v1

obtained from https://rda.ucar.edu/datasets/ds316.1 [41]. This future day initial and boundary condition information is spaced at 1^0 x 1^0 resolution. In the support of Coupled Model Intercomparison Experiment Phase 5 (CMIP5) [42] and the Intergovernmental on Climate Change Fifth Assessment Report [43], the CESM simulations, therefore, were utilized to produce future-day simulation which has a better agreement in simulating temperature and precipitation globally compared to real-time observation [44]. The future simulation carried out under the three climate change scenarios is also known as Representative Concentration Pathways (RCPs) from AR5 IPCC [43]. The first future scenario of RCP4.5 is a low-to-moderate emission scenario, where the greenhouse gases (GHGs) radioactive forcing will reach 4.5 Wm^{-2} by the year 2100 [45]. It represents a scenario where a variety of adaptive policies has been applied to limit the radiative forcing. Besides that, the medium-range RCP6.0 will be stabilizing without overshoot pathway to 6 Wm^{-2} at stabilization after 2100 [46]. RCP8.5 indicates a high emission scenario with GHGs radiative forcing that will reach 8.5 Wm^{-2} by the year 2100 [47].

2.2.2. Biogenic Model

In this research, the Model of Emission Gases and Aerosols from Nature Version 2.1 (MEGAN V2.1) which was originally written by Guenther [48-49] and available at https://bai.ess.uci.edu/megan was used to quantify the net emission rate of biogenic emission between the atmosphere and terrestrial ecosystem. The model simulates the total biogenic emission at a specific location and time, while considering the impact meteorology (e.g., hourly temperature, solar radiation, humidity, wind speed and soil moisture), land cover and plant functional type. Details of the biogenic emission process is calculated using the following equation.

$$\text{Biogenic Emission} = [\varepsilon][\ \gamma][\rho], \quad (1)$$

MEGAN is designed to simulate the net emissions of gases and aerosols into the atmosphere from terrestrial ecosystems [48]. It is primarily designed for both global and regional emissions modelling with a spatial spaced up to 1 km resolution. MEGAN is a semi-mechanistic model that takes into account the major known processes that control biogenic emissions. MEGAN only estimates emissions of known compounds which includes 150 chemical species. These 150 compounds are lumped into 20 categories based on how emissions vary in response to changes of driving variables such as land cover, weather, and atmospheric chemical composition.

Emission Factor at the Canopy-Scale ($\boldsymbol{\varepsilon}$) or emission rate is a weighted average of the canopy emission factor for each vegetation type. γ is a normalized emission activity factor to explain changes caused by deviations from standard conditions in environmental variables. Meanwhile, ϱ is the standardized factor for explaining variations in chemical production and loss in plant canopies compared to standard conditions that is equal to 1. While γ is dependent on the environmental and climatic factors as described by [48] in the following equation.

$$\gamma = \gamma_{CE} \times \gamma_{age} \times \gamma_{SM} \quad (2)$$

Where, $\boldsymbol{\gamma_{CE}}$ describes variation due to Leaf Area Index (LAI) and light, temperature, humidity, and wind conditions within the canopy environment, $\boldsymbol{\gamma_{age}}$ makes adjustments for effects of leafage, and $\boldsymbol{\gamma_{SM}}$ accounts for the direct change in $\boldsymbol{\gamma}$ due to changes in soil moisture. The calculation of each of these factors is described in the study of [48]. Local climatic conditions, which affect the incident PPFD and leaf temperature, are known to control the biogenic emission such as isoprene from short periods (seconds to minutes) to longer periods (hours to weeks) of time scales [50-51].

The driving data for MEGANv2.1 includes vegetation and meteorological information. Vegetation data includes PFT and LAI. This study used the CLMv4 dataset available at https://svn-ccsm-inputdata.cgd.ucar.edu/trunk/inputdata/ for PFT and MODIS LAI collection 5 product [52] to simulate the biogenic emission over SEA region. There are

Preprints (www.preprints.org) | NOT PEER-REVIEWED | Posted: 22 March 2023 doi:10.20944/preprints202303.0394.v1

16 plant functional types under CLM4 namely 3 Needleleaf, 8 Broadleaf, 3 grass, and 2 corps which were then mapped under MEGAN v2.1. The LAI dataset has a time interval of 8-day. Thus, there are 4 LAI datasets for each period of the study (i.e., July 4th, 12th, 20th and 28th). Both PFT and LAI data have a spatial resolution of 500 m. Before being used in this study, we first resampled them to a resolution of 0.04°. The meteorological data as parameterized input that affects the emission environment (e.g., solar radiation, temperature, relative humidity, and soil moisture) [53] for this study is provided by the WRF model.

2.2.3. Model Simulation

The WRF and MEGAN model under this study was run with one-hour temporal resolution and 25 km x 25 km spatial resolution. The year 2013 was selected as the baseline year of the present-day simulation, and the future projection is in the years 2030, 2050, 2070, and 2100. The simulation was carried out in January (representing winter monsoon) and July (representing summer monsoon) of the selected time slice. For January, the projection time began at 0000 UTC of first January and ended at 0000 UTC first February. While for July, the projection time began at 0000 UTC of first July and ended at 0000 UTC first August.

2.2.4. Climate Change Impact on Biogenic Emission

Changes of temperature might be the main driver of biogenic emissions [54]. In general, the BVOC emission profile increases gradually with the increase of temperature as it increases the plant's synthase activity [14]. Plant synthase volatile compound to stabilize cell membrane during high temperature as a thermotolerance mechanism [55]. An increase of temperature above 30 °C leads to an increase of BVOCs emission by two to eight times [56-58]. The exponential dependence of BVOC emissions on increasing temperature has also been well documented in the prior work of Guenther [48]. Besides temperature, one of the most regarded factors impacting plant photosynthesis, and thus BVOC emission, is light availability. PAR (photosynthetic active radiation) is the part of the visible spectrum (0.4–0.7 μm) that stimulates photosynthesis by activating chlorophyll in plants. Isoprene particularly is very sensitive to the changes in PAR [2] and was reported to increase the emission rate by 50% for some species when the PAR level was double at a temperature above 30 °C [59].

Higher temperature will lead to an increase in enzyme activity, transcriptional levels, and synthetase rate. PAR is more effective at increasing plants' photosynthesis than direct light [60]. In this study, we highlight the effect of both temperature and PAR under climate change scenario of RCP4.5 and RCP8.5 on biogenic emission during both the January and July period.

3. Results

3.1 Climate change simulation

3.1.1 Surface temperature

The regional climate simulations over the SEA region during January and July for the baseline period of 2013, future period years 2030 (near mid-century), 2050 (mid-century), 2070 (post-mid-century), and 2100 (end of the century) under the three RCPs are shown in the Figure 2 (RCP4.5), Figure 3 (RCP4.5) and Figure 4 (RCP8.5). Based on the projected simulation by the WRF model, the mean surface temperature for the projected period (2013, 2030, 2050, 2070, and 2100) was projected at average of 22.9°C, 22.5°C, 23.5°C, 23.3°C

Preprints (www.preprints.org) | NOT PEER-REVIEWED | Posted: 22 March 2023 doi:10.20944/preprints202303.0394.v1

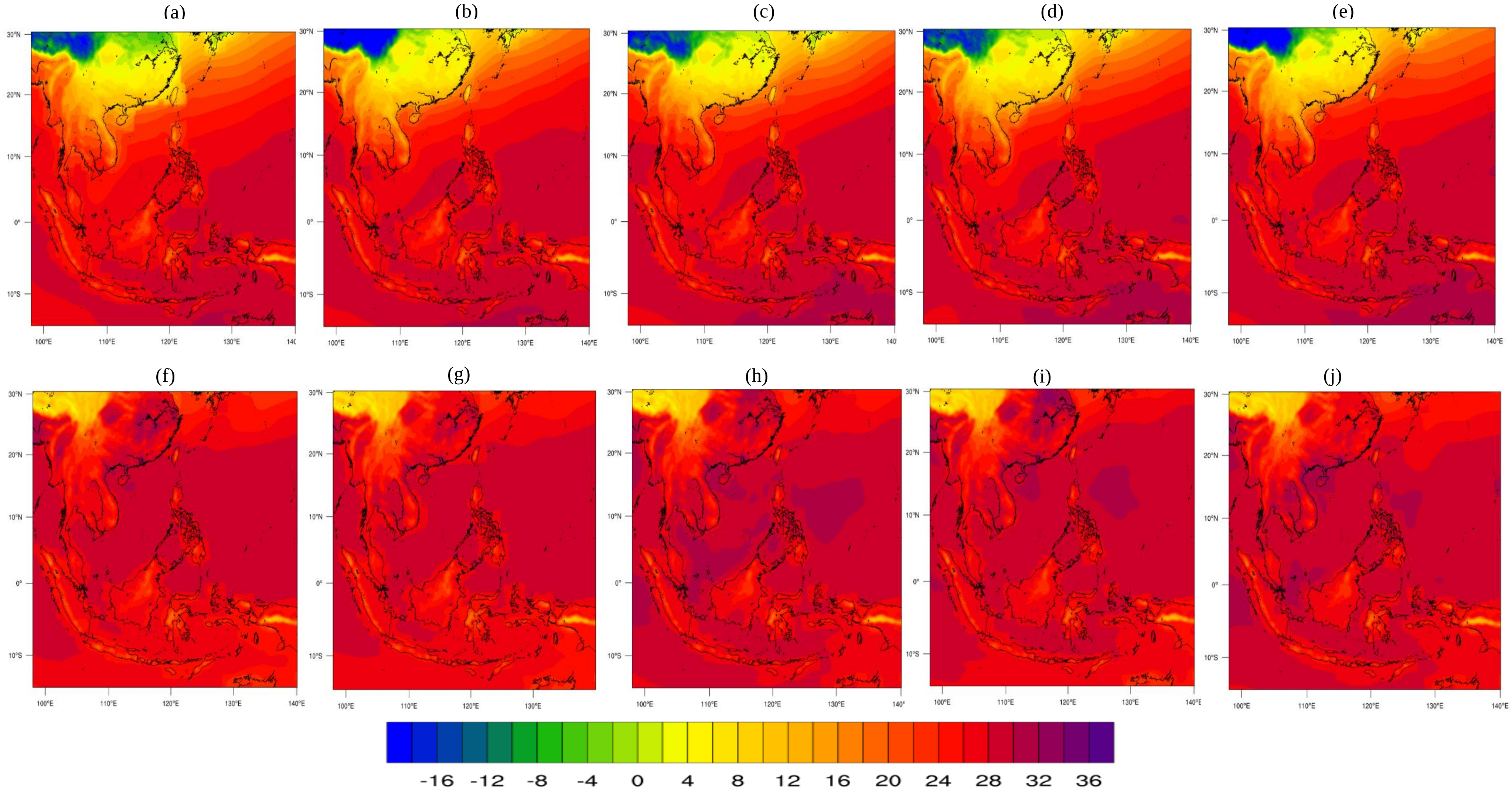

Figure 2. Mean surface temperature for SEA region under RCP4.5 during January of 2013 (a), 2030 (b), 2050 (c), 2070 (d) and 2100 (e); and on July of 2013 (f), 2030 (g), 2050 (h), 2070 (i), and 2100 (j).

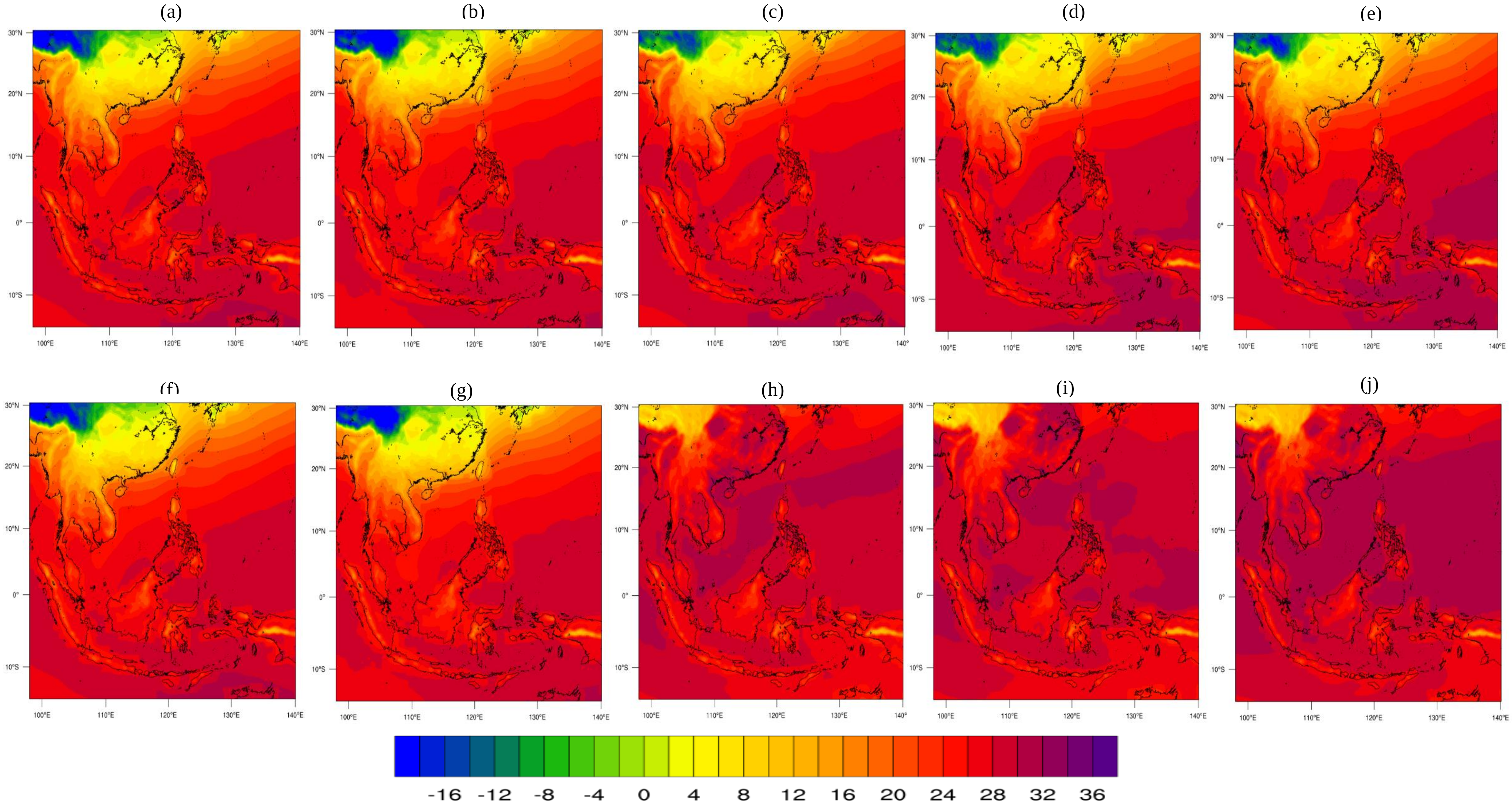

Figure 3. Mean surface temperature for SEA region under RCP6.0 during January of 2013 (a), 2030 (b), 2050 (c), 2070 (d) and 2100 (e); and on July of 2013 (f), 2030 (g), 2050 (h), 2070 (i), and 2100 (j).

Preprints (www.preprints.org) | NOT PEER-REVIEWED | Posted: 22 March 2023 doi:10.20944/preprints202303.0394.v1

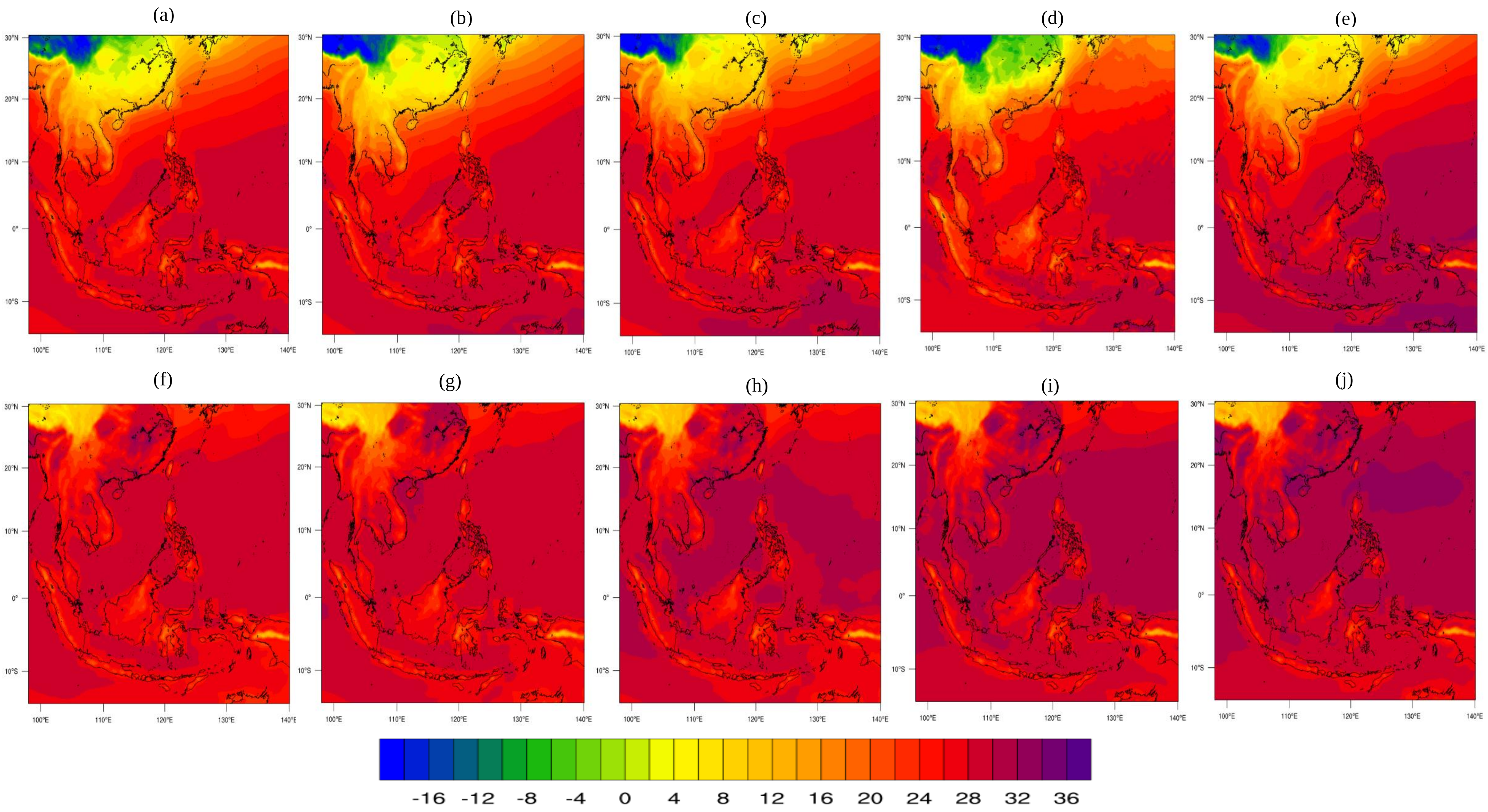

Figure 4. Mean surface temperature for SEA region under RCP8.5 during January of 2013 (a), 2030 (b), 2050 (c), 2070 (d) and 2100 (e); and on July of 2013 (f), 2030 (g), 2050 (h), 2070 (i), and 2100 (j).

and 23.7℃ throughout January. Whereas in July RCP4.5, the mean temperatures are 26.7℃, 26.9℃, 27.4℃, 27.2℃, and 27.7℃. Overall, there is an average increment of 0.6℃ in January and 0.7℃ in July, during mid of century which is pronounced (with >1.5℃) over the mainland SEA (MSEA) region of Cambodia, Laos, Myanmar, Thailand, and Vietnam relative to the baseline period (2013). Towards the end of the century, the increment is more significant at an average of 0.8℃ and 1.0℃ for both January and July. However, the temperature increment over the MSEA region is projected to become less pronounced at the end of the century despite a steady increase simulated for the insular region (Malaysia, Indonesia, and the Philippines).

Under RCP6.0, the projected mean temperature over the SEA region for January of 2013, 2030, 2050, 2070, and 2100 are 22.4℃, 23.2℃, 24.1℃, 23.5℃, and 24.1℃, respectively. Whereas in July, the regional mean surface temperatures are 26.5℃, 26.8℃, 27.4℃, 27.7℃, and 28.2℃ (Figure 3). Towards the mid of century, the mean surface temperature is projected to increase by 1.7℃ in January and 0.9 in July relative to the baseline period. While for January and July at the end of century, both projected surface temperatures are projected to remain at the rate of 1.7℃. Despite the significant increase of temperature in January over MSEA until the mid-century under this RCP, the insular region is expected to experience less significant temperature increment towards the end of century similar to RCP4.5.

The RCP8.5 scenario suggests a higher mean temperature in both January and July throughout the projected periods. The average mean surface temperature for January for the years 2013, 2030, 2050, 2070, and 2100 are 23.3°C, 23.0°C, 23.1°C, 24.7°C, and 25.4°C. While for the same time slice in July, the mean surface temperatures are 26.6°C, 27.4°C, 27.6°C, 28.1°C, and 29.1°C, respectively (Figure 4). There is a decrement in regional average temperature by -0.20℃ in January; however, the average temperature increased by 0.99℃ in the mid of century. At the end of the century, a higher increment of temperature is noticeable by 2.1℃ in January and 2.50℃ in July. Though the MSEA has a lower mean temperature in January but higher in July, the mean temperature in the insular region for both January and July gradually increase towards the end of the century.

Despite the discrepancy in surface temperature projection under the different RCPs, there is an agreement between climate scenarios that at the mid of century, the maritime region of SEA will experience a warmer climate at 0.4°C – 1.2°C under RCP4.5, 0.8°C – 1.4°C under RCP6.0, and 0.4°C – 1.0°C under RCP8.5. Similarly, the result of simulation for all the RCPs agrees that there is additional warming over the MSEA between 1.3°C – 1.5°C under RCP4.5, 1.1°C – 2.1°C under RCP6.0, and 2.0°C – 2.5°C under RCP8.5 subsequently. The result is almost similar to the finding of Supharatid [61] which used CORDEX-SEA, and projected warming that is more pronounced in the boreal summer season over MSEA with an increment of about 1.2℃ - 2.0℃ during mid of century, and 1.2℃ - 2.0℃ at the end of century. However, the work based on CORDEX-SEA was unable to resolve a more precise simulation with a bias of 2.5℃ and coarser grid resolution. Moreover, the difference between the results arises from the variance scaling method, simulation periods, and the model's internal forcing [62]. Likewise, Thirumalai [63] stated that the warming in SEA is higher than the global average especially during the El Nino event. Meanwhile, Raghavan [64] and Gasparrini [65] suggested that the mean surface temperature is likely to further increase by more than 3.5℃ during the end of the century for this region.

3.1.2 PAR

Figures 5, 6, and 7 show the average PAR from the WRF model during both the January and July periods for the years 2013, 2030, 2050, 2070, and 2100 under all three RCPs. Overall, the mean simulated PAR for the January period of 2013, 2030, 2050, 2070, and 2100 are 303.76 W m^{-2}, 305.34 W m^{-2}, 307.31 W m^{-2}, 308.93 W m^{-2}, and 308.21 W m^{-2}, respectively. While in July, the simulated average PAR value was higher with values of 330.78

 doi:10.20944/preprints202303.0394.v1

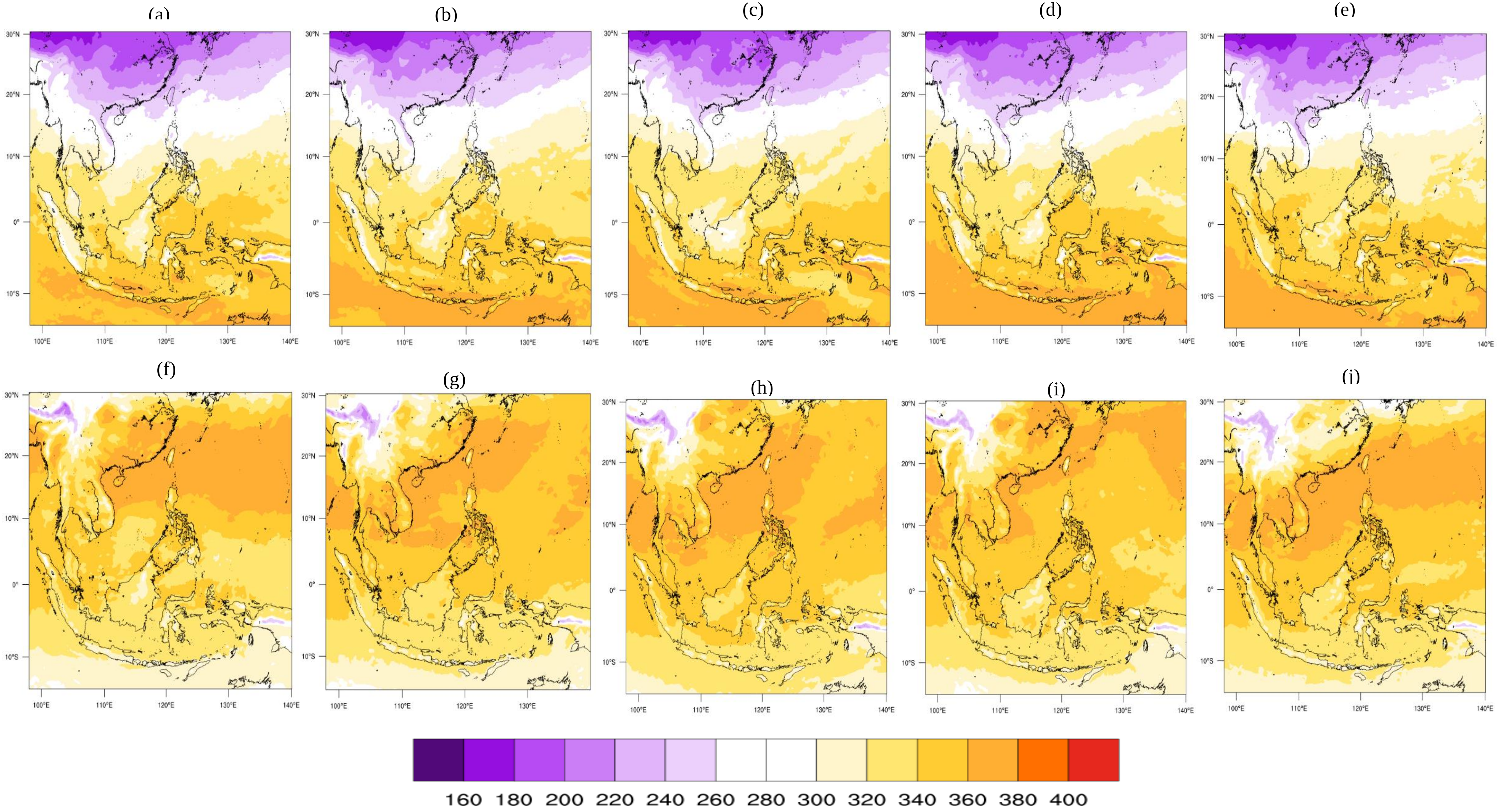

Figure 5. Mean PAR for SEA region under RCP4.5 during January of 2013 (a), 2030 (b), 2050 (c), 2070 (d) and 2100 (e); and on July of 2013 (f), 2030 (g), 2050 (h), 2070 (i), and 2100 (j).

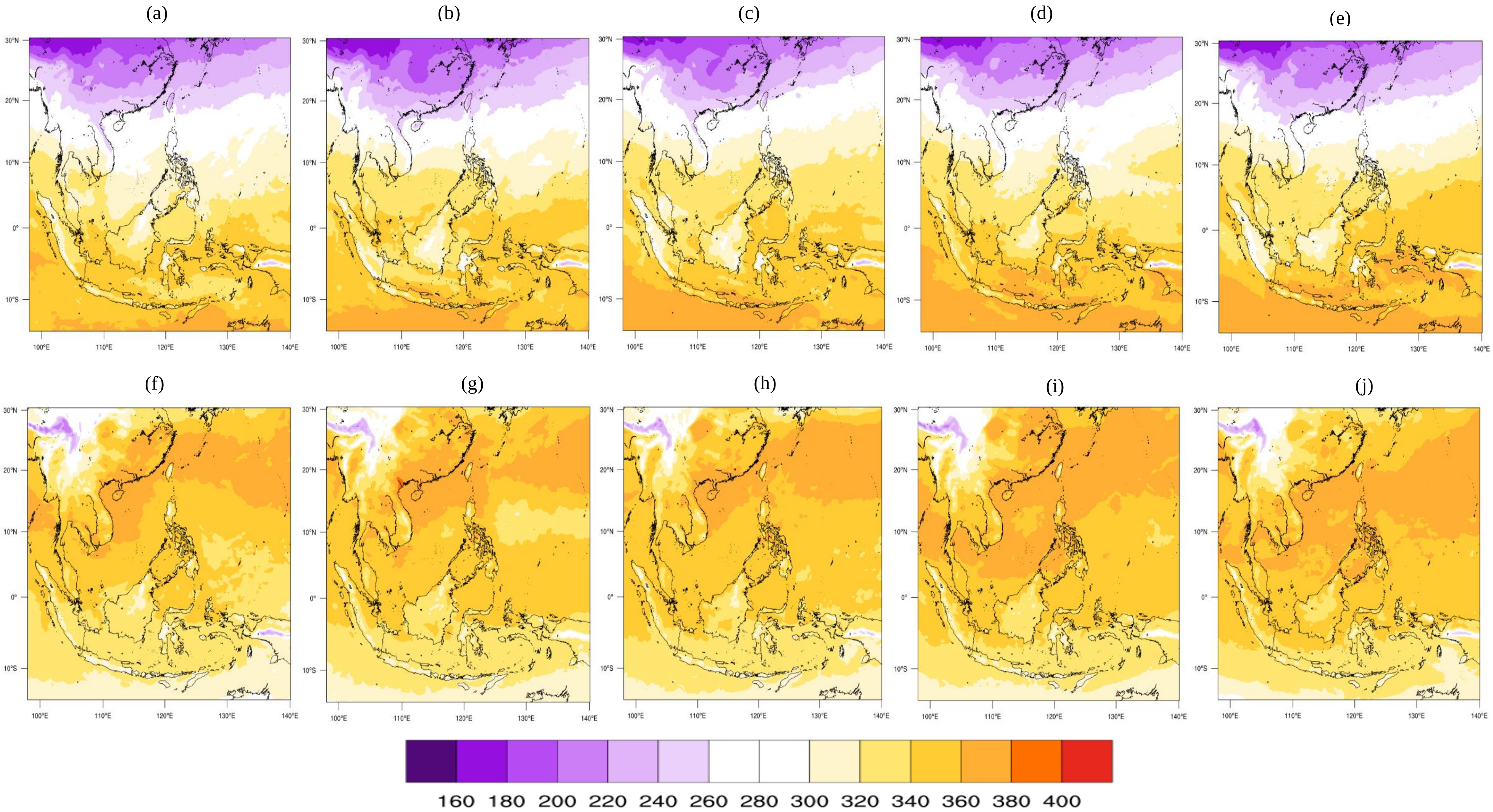

Figure 6. Mean PAR for SEA region under RCP6.0 during January of 2013 (a), 2030 (b), 2050 (c), 2070 (d) and 2100 (e); and on July of 2013 (f), 2030 (g), 2050 (h), 2070 (i), and 2100 (j).

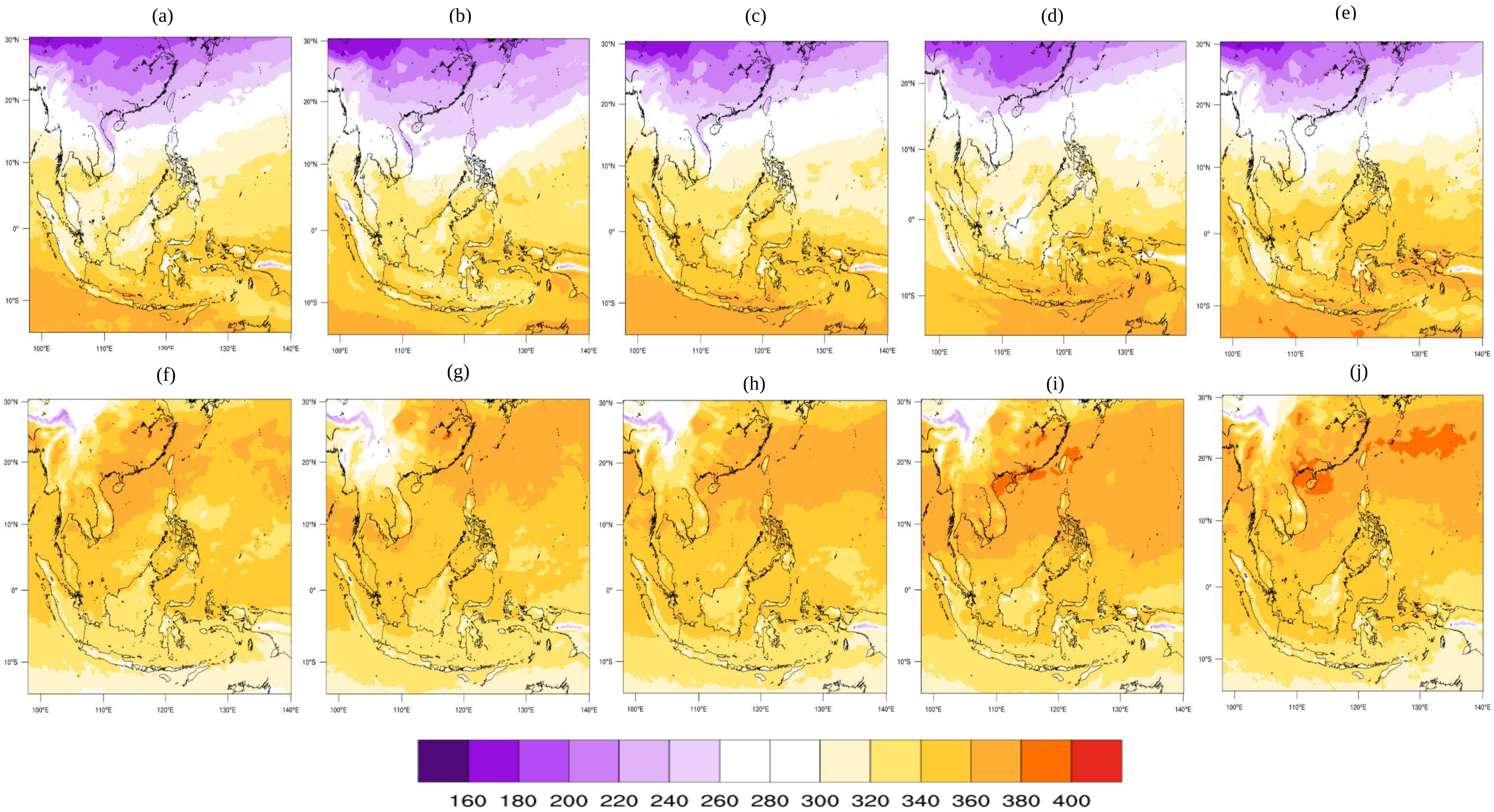

Figure 7. Mean PAR for SEA region under RCP8.5 during January of 2013 (a), 2030 (b), 2050 (c), 2070 (d) and 2100 (e); and on July of 2013 (f), 2030 (g), 2050 (h), 2070 (i), and 2100 (j).

W m-2, 333.34 W m-2, 335.67 W m-2, 334.01 W m-2, and 334.30 W m-2, respectively (Figure 5). The RCP4.5 result depicts that there is an increment of PAR during both periods of study with an average of 3.55 W m-2 and 4.89 W m-2 towards the mid of century, and 4.45 W m-2 and 3.52 W m-2 at the end of century.

Whereas under RCP6.0 (Figure 6) and RCP8.5 (Figure 7), the results of the WRF simulation of mean PAR over the domain of study are 303.27 W m^{-2}, 303.62 W m^{-2}, 308.79 W m^{-2}, 309.25 W m^{-2} and 310.86 W m^{-2} during January, and 331.98 W m^{-2}, 334.24 W m^{-2}, 335.53 W m^{-2}, 337.20 W m^{-2} and 338.51 W m^{-2} during July of the selected time slice. The simulated PAR under RCP8.5 projection shows an even higher value with an average of 304.72 W m^{-2}, 302.47 W m^{-2}, 308.31 W m^{-2}, 302.08 W m^{-2}, and 311.63 W m^{-2} for January, and 332.13 W m^{-2}, 334.70 W m^{-2}, 336.36 W m^{-2}, 341.99 W m^{-2}, and 340.93 W m^{-2} for July. Relatively, these results suggest that the highest increment of PAR in January is observed under RCP6.0 over the domain of study with a value of 5.07 and 7.59 towards the mid and end of century, respectively. The highest PAR increment in July towards the mid and end of century are observed under RCP8.5 with an increment rate of 4.23 W m^{-2} and 8.80 W m^{-2}.

Compared to the simulated surface temperature, the changes of PAR are relatively less visible for both MSEA and insular region, thus scattering all over the region. However, the MSEA region experienced higher transitions of PAR changes from January to July. A similar finding over the whole SEA domain was also found in the study of [66] who also simulated a net increase of projected radiation at the end of century with an average of 3.1 W m^{-2} and 3.8 W m^{-2} for winter (January) and summer (July), respectively. Moreover, this finding particularly over Malaysia and the Borneo Island region, is also in agreement with the study of Kong [67], who simulated a higher radiation during the January and July period with increments of 7.40 W m^{-2} – 12.40 W m^{-2} under RCP4.5 and 26.20 W m^{-2} – 45.70 W m^{-2} under RCP8.5. Owing to the difference between climate simulation techniques, the model's internal forcing, simulation period, and interpolation method, the difference in simulation of the net surface temperature and PAR change might also be hampered by a poor topography precision and land use setting, particularly in areas with complex topographic and land use distribution [62].

3.2 *Isoprene emission under climate change scenario*

The projected isoprene emissions in SEA under RCP4.5 for 2013, 2030, 2050, 2070, and 2100 are shown in Figure 8. The projected isoprene emissions in January are found at 0.252 tons/hr in 2013, 0.249 tons/hr in 2030, 0.266 tons/hr in 2050, 0.289 tons/hr in 2070, and 0.288 tons/hr in 2100. In July, the average isoprene emissions are 0.315 tons/hr in 2013, 0.329 tons/hr in 2030, 0.344 tons/hr in 2050, 0.339 tons/hr in 2070, and 0.345 tons/hr in 2100. The results revealed an increasing trend of projected isoprene emissions rate towards the end of the century for this region with 1.2% – 14.3% in January and 4.4% – 9.5% in July.

The projected isoprene emissions under RCP6.0 (Figure 9) were higher than the RCP4.5 scenario, with total projected emission rates in January of 0.252 tons/hr, 0.257 tons/hr, 0.264 tons/hr, 0.294 tons/hr, and 0.291 tons/hr for the years 2013, 2030, 2050, 2070 and 2100. The increment of isoprene emission in SEA was recorded at a range of 1.9% – 15.5% from near-mid and towards the end of century, respectively. In July, the average isoprene emissions are 0.304 tons/hr in 2013, 0.351 tons/hr in 2030, 0.354 tons/hr in 2050, 0.369 tons/hr in 2070, and 0.396 tons/hr in 2100. Similarly, a higher increment rate was found under this RCP with 15.5 % – 30.3% from near-mid and towards the end of century, respectively.

Under the RCP8.5 scenario, the total isoprene emissions are projected with an increasing trend in both January and July (Figure 10). In January, the projected average isoprene emissions are 0.229 tons/hr in 2013, 0.252 tons/hr in 2030, 0.274 tons/hr in 2050, 0.333 tons/hr in 2070, and 0.352 tons/hr in 2100. Whereas in July for the same time slice, the projected average isoprene emissions are 0.336 tons/hr, 0.328 tons/hr, 0.362 tons/hr, 0.413 tons/hr, and 0.433 tons/hr, respectively. The changes in future projections of isoprene emissions towards the end of century relative to the baseline period were more significant

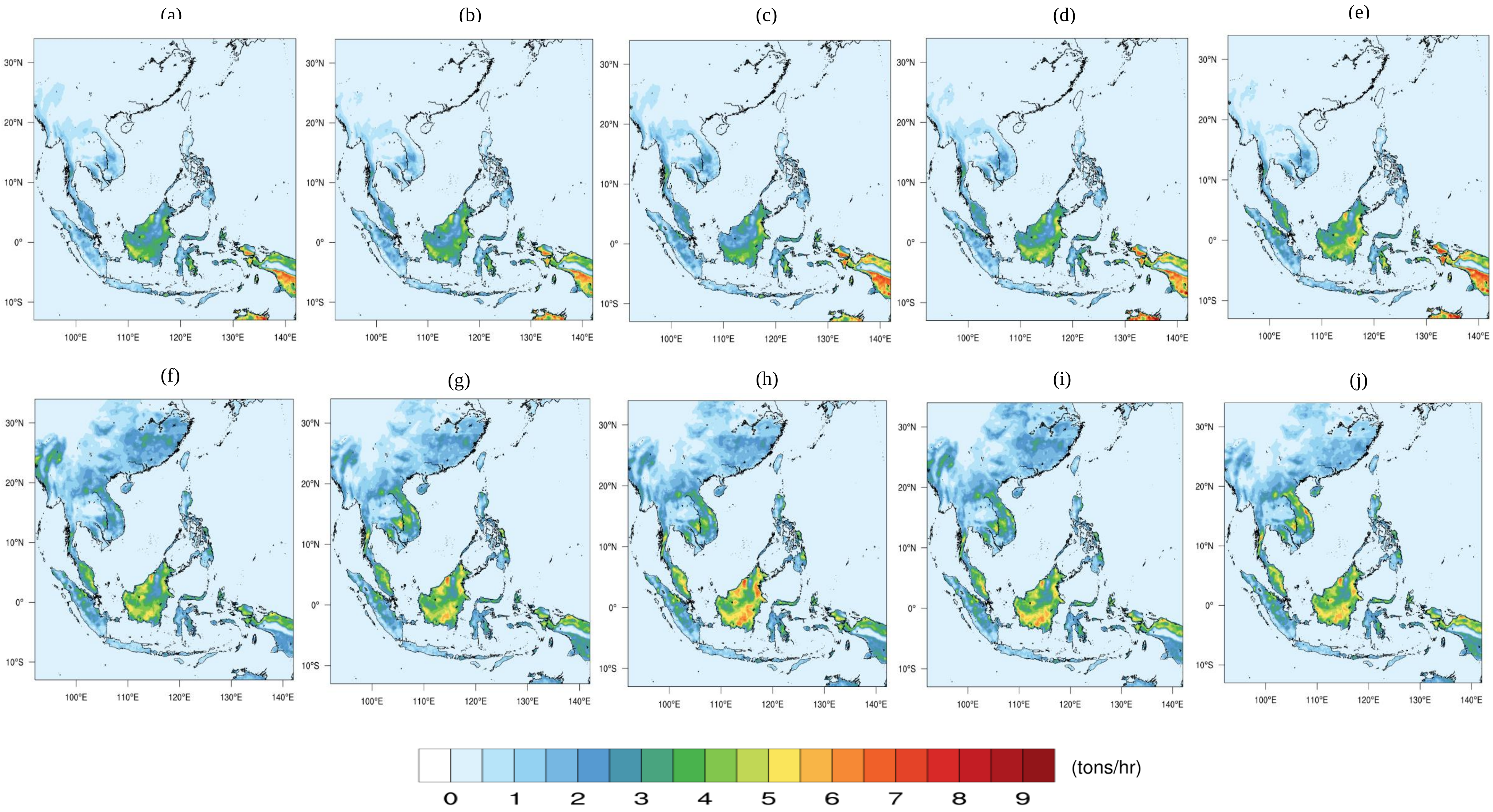

Figure 8. Mean isoprene emission for SEA region under RCP4.5 during January of 2013 (a), 2030 (b), 2050 (c), 2070 (d) and 2100 (e); and on July of 2013 (f), 2030 (g), 2050 (h), 2070 (i), and 2100 (j).

Preprints (www.preprints.org) | NOT PEER-REVIEWED | Posted: 22 March 2023 doi:10.20944/preprints202303.0394.v1

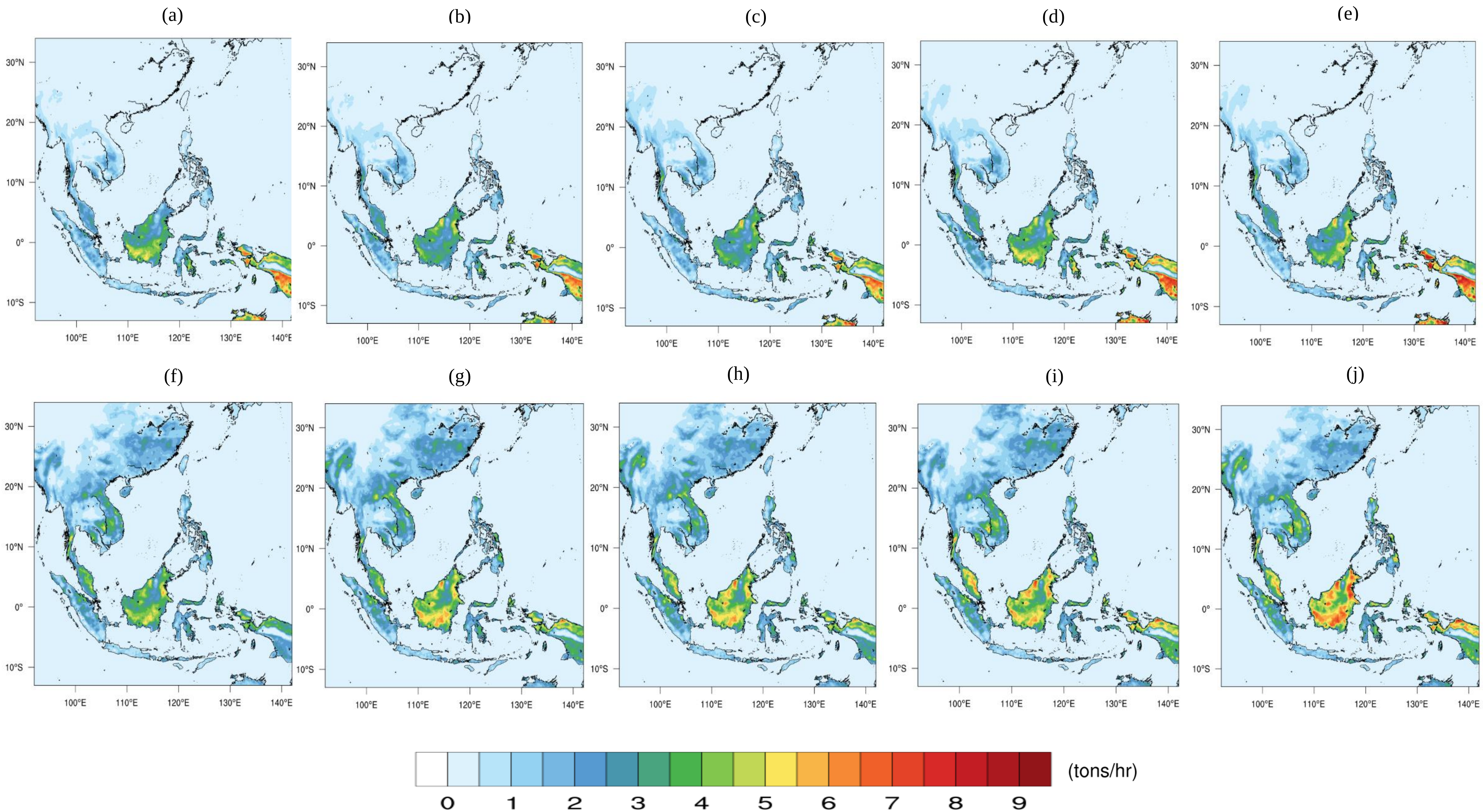

Figure 9. Mean isoprene emission for SEA region under RCP6.0 during January of 2013 (a), 2030 (b), 2050 (c), 2070 (d) and 2100 (e); and on July of 2013 (f), 2030 (g), 2050 (h), 2070 (i), and 2100 (j).

Preprints (www.preprints.org) | NOT PEER-REVIEWED | Posted: 22 March 2023 doi:10.20944/preprints202303.0394.v1

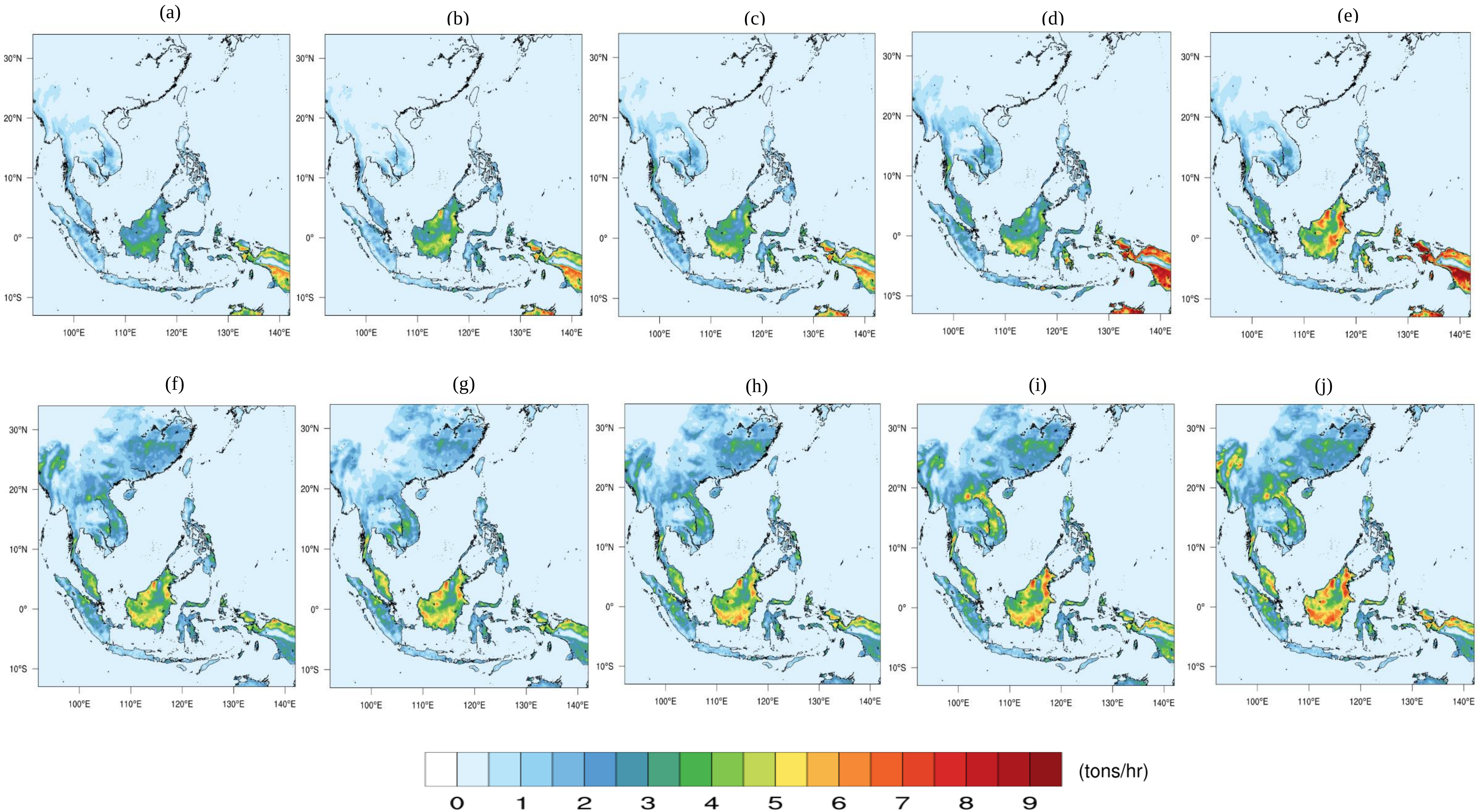

Figure 10. Mean isoprene emission for SEA region under RCP8.5 during January of 2013 (a), 2030 (b), 2050 (c), 2070 (d) and 2100 (e); and on July of 2013 (f), 2030 (g), 2050 (h), 2070 (i), and 2100 (j).

than RCP4.5 and RCP6.0 with increments of 10.0% - 53.7% and 7.7% - 28.9% for January and July, respectively.

4. Discussion

As shown in Figure 8, the projected RCP4.5 isoprene simulation in January shows that the all-time high isoprene emitter is within the Borneo, Sulawesi, and Papua Island region. Malaysia and Indonesia are the main oil palm producers in SEA [68] with isoprene emissions of five times greater than the primary tropical forest landscapes [69]. Thus, the projected emissions of isoprene in Malaysia and Indonesia are consistently higher than that of other countries. Meanwhile, the lowest emitters are within the mainland of SEA, such as Myanmar, Laos, and Vietnam with no significant changes of emission throughout the study. The low emission in MSEA is modulated by low temperature (whereby temperatures become colder towards the end of the century in January) which could suppress the emission of isoprene [70-71].

The large modulation of total isoprene emission in MSEA during both periods of July might also be associated with PAR. It is worth mentioning that the isoprene emission, temperature, and PAR move at the same trend towards the end of the century. This finding is in agreement with the prior study of [72-76] which highlighted that the isoprene emission had indeed increased due to elevated temperature and total radiation. Therefore, the increased emission rate in July for the MSEA region and Borneo was due to the increase of temperature and PAR, while the low isoprene emission observed over Papua Island is aligned with the lower mean simulated PAR and temperature under the RCP4.5 climate scenario projection.

The projected isoprene emission in January under RCP6.0 also showed that the all-time highest isoprene emitter is also in the region of Borneo, Sulawesi, and Papua Island. Similar to the RCP4.5 scenario, the mainland SEA region has the lowest emission rate but with noticeable shift in July especially in Laos, Cambodia, and Vietnam. The noticeable shift was also marked by a significant shift in mean temperature and PAR observed for these regions. This finding further supports that the isoprene emission for these regions may be strongly influenced by the climatic (temperature and PAR) factors. There is corresponding evidence of the isoprene emission distribution among plant species, and it was generally agreed that the emission increases under high-temperature episodes [17,77-79].

It was observed that both the Borneo and Papua Island region underwent a noticeable shift in isoprene emission from January to July for all the time slices. Likewise, the increment of isoprene emission in Borneo from January to July was also followed by the increase in temperature and PAR. Since both temperature and PAR are lower in July than in January, the projected isoprene emission in July over Papua Island was lower than in January for the time slices. Thus, it is further expected that the noticeable change in isoprene emission under the RCP6.0 simulation is also highly related to the changes of temperature and PAR simulated in the WRF model, though other abiotic stressors such as water stress and drought could also potentially suppress the photosynthesis rate therefore buffering the isoprene emission rate [54,56,80-81].

Similarly, the projected isoprene simulations in January and July under RCP8.5 also showed that the all-time highest isoprene emitter is also distributed in the region of Borneo and Papua Island. Overall, the projected total isoprene emissions for both mainland and insular regions move on the same trend with the changes of total mean temperature and PAR, and the increase was more noticeable after mid of century, hence reflecting the whole point of which plant emits more isoprene emission to sustain a warmer temperature and higher exposure of sunlight [15,21,35,54,59,82-84].

The projected simulation of isoprene emissions in July revealed a transient increase of total isoprene emissions, especially over the MSEA region. It is noteworthy that the significant increase of isoprene emission over MSEA in July was marked by the surface temperature which persists at 25 – 30 °C during mid-century, 30 – 34 °C afterwards, and increased PAR of more than 8 W m^{-2}. As mentioned in the literature insertion of Mu [85], the emission rate of isoprene from plant increases to better tolerate higher steady-state of temperature and higher cumulative exposure of solar radiation (especially in July or warmer season) [54,71,79]. Thus, the finding of this study on the relationship between isoprene and changing climate (temperature and PAR) is similar to the finding of the aforementioned prior and recent studies.

5. Conclusions

The climate model simulation projected that the average temperatures over SEA are 22.88°C – 26.66°C, 22.4°C – 26.5°C, and 23.3°C – 26.6°C for the baseline period under RCP4.5, RCP6.0, and RCP8.5, respectively. Towards the mid-century, this region is expected to experience surface temperature anomaly at an average of 0.6°C – 0.8°C under RCP4.5, 0.9°C – 1.6°C under RCP6.0, and 0.2°C – 1.0°C under RCP8.5. At the end of the century, this region is projected to have a warmer climate with temperature increments at an average of 0.8°C – 0.9°C under RCP4.5, 1.6°C – 1.7°C under RCP6.0, and 2.1°C – 2.5°C under RCP8.5. The surface temperature anomaly for all the RCPs is more pronounced over MSEA (Myanmar, Thailand, Cambodia, Laos, and Vietnam) with an average projected increment of 2.0°C – 6.0°C for both periods towards the end of century. Meanwhile, the insular region has a lower temperature anomaly ranging from 2.0°C – 4.0°C.

The WRF simulation of mean PAR for RCP4.5, RCP6.0, and RCP8.5 over the domain of the study ranged from 303.76 W m^{-2} - 334.30 W m^{-2}, 303.27 W m^{-2} - 338.51 W m^{-2}, and 302.47 W m^{-2} - 340.93 W m^{-2}, respectively. Higher transition of PAR from January to July (with an increment of 15 W m^{-2} – 18 W m^{-2}) was observed over the MSEA region for all the time slices. It is hence concluded that in July, the Papua Island experienced a reduction in PAR (at an average of 7.6 W m^{-2} – 12 W m^{-2} for all the RCPs) towards the end of century. The finding also depicts that there is an increment of PAR during both periods of study ranging from 3.55 W m^{-2} - 7.59 W m^{-2} during mid of century and from 3.52 W m^{-2} – 8.80 W m^{-2} towards the end of century.

Both the higher temperature and PAR transition from January to July are contributed by seasonal monsoon changes as discussed in the study of [86]. During winter monsoon period (from December to February), the tilting of the Earth allows less solar radiation in the northern hemisphere hence leading to less radiation over MSEA. This results in rapid cooling followed by a pressure decrease in the atmosphere. The tilting of the earths and the ocean-atmosphere interaction can be a source of climate variability and of which shapes the dynamics of the regional monsoon system, hence influencing the changes in temperature and PAR over this region.

Based on the projected results from the MEGAN model, the total isoprene emissions estimated over the SEA region are 0.252 – 0.315 tons/hr, 0.252 – 0.304 tons/hr, and 0.229 – 0.336 tons/hr for the baseline period under RCP4.5, RCP6.0, and RCP8.5, respectively. During the mid of century, the isoprene emissions during January and July suggest an increment of about 5 – 9% in RCP4.5, 5 – 16% under RCP6.0, and 8 – 20% under RCP8.5. At the end of the century, the projected increment of isoprene emissions over this region are at 10 – 14%, 15-30%, and 29 – 53% for RCP4.5, RCP6.0, and RCP8.5, respectively. The finding also revealed that the all-time high emission region is Borneo and Papua Island, with an average emission rate of 2-4 tons/hr under RCP4.5, 2-6 tons/hr under RCP6.0, and 2-8 tons/hr under RCP8.5.

Towards the end of century, all climate-biogenic simulation agrees that in July, the region emits more isoprene than in January. The finding showed that isoprene emission will increase due to the increase in temperature and PAR, and the seasonal differences between the isoprene emission rates are also correlated to the seasonal differences in PAR and temperature value. Although the entire region showed increasing isoprene emission rates in July, the emission rate over Papua Island showed a decreasing rate due to a reduction of PAR despite the increasing temperature towards the end of century.

However, the whole process of simulation under this study kept the anthropogenic emission at the present level (2013 period) to isolate the effect of climate change alone. The general isoprene emission can be affected by multiple factors due to the complex interaction of meteorological and atmospheric chemistry. Apart from surface temperature and PAR, the impact of drought, soil moisture, and bio-physiochemical interaction between isoprene and CO_2 as well as between isoprene and land cover changes are needed to generate better ideas of isoprene changes in the future.

Funding: This research was partially funded by Asia Pacific Network Research Grant (APN), grant number CRRP2017-02MY. The authors alone are responsible for the content, which does not reflect the official viewpoints of the Asia Pacific Network organization.

References

1. Loreto, F.; Dicke, M..; Schnitzler, J.P.; Turlings, T.C. Plant volatiles and the environment. *Plant, cell & environment*, **2014**, 37(8), pp. 1905-1908.
2. Guenther, A.B.; Jiang, X.; Heald, C.L.; Sakulyanontvittaya, T.; Duhl, T.; Emmons, L.K.; Wang, X. The Model of Emissions of Gases and Aerosols from Nature version 2.1 (MEGAN2. 1): an extended and updated framework for modeling biogenic emissions. *Geoscientific Model Development*, **2012,** 5(6), pp. 1471-1492.
3. Lin, Y.; Lun, X.; Tang, W.; Zhang, Z.; Jing, X.; Fan, C.; Wang, Q. Characteristics and chemical reactivity of biogenic volatile organic compounds from dominant forest species in the Jing-Jin-Ji area, China. *Forest Ecosystems*, **2021,** 8(1), pp. 1-14
4. Li, S.J.; Yuan, X.Y.; Li, Q.; Feng, Z.Z. Inventory and characteristics of biogenic volatile organic compounds (BVOCs) for 12 deciduous fruit trees. *Huan jing ke xue= Huanjing kexue*, **2019,** 40(5), pp.2078-2085.
5. Lim, C.C.; Hayes, R.B.; Ahn, J.; Shao, Y.; Silverman, D.T.; Jones, R.R.; Garcia, C.; Bell, M.L.; Thurston, G.D. Long-term exposure to ozone and cause-specific mortality risk in the United States. *American journal of respiratory and critical care medicine*, **2019,** 200(8), pp. 1022-1031.
6. Fowler, D.; Pilegaard, K.; Sutton, M.A.; Ambus, P.; Raivonen, M.; Duyzer, J.; impson, D.; Fagerli, H.; Fuzzi, S.; Schjoerring, J.K.; Granier, C.; and Erisman, J.W. Atmospheric composition change: ecosystems–atmosphere interactions. *Atmospheric Environment*, **2009**, 43(33), pp. 5193-5267.
7. Kumar, P.; Imam, B. Footprints of air pollution and changing environment on the sustainability of built infrastructure. *Science of The Total Environment*, **2013**, 444, pp. 85-101.
8. Malkina, I.L.; Kumar, A.; Green, P.G.; Mitloehner, F.M. Identification and quantitation of volatile organic compounds emitted from dairy silages and other feedstuffs. *Journal of environmental quality*, **2011**, 40(1), pp. 28-36.
9. Crespo, E.; Graus, M.; Gilman, J.B.; Lerner, B.M.; Fall, R.; Harren, F.J.M.; Warneke, C. Volatile organic compound emissions from elephant grass and bamboo cultivars used as potential bioethanol crop. *Atmospheric Environment*, **2013**, 65, pp. 61-68.
10. Davis, T.S.; Crippen, T.L.; Hofstetter, R.W.; Tomberlin, J.K. Microbial volatile emissions as insect semiochemicals. *Journal of chemical ecology*, **2013**, 39(7), pp. 840-859.
11. Loreto, F.; Schnitzler, J.P. Abiotic stresses and induced BVOCs. *Trends in plant science*, **2010,** 15(3), pp. 154-166.
12. Tani, A.; Mochizuki, T. Exchanges of volatile organic compounds between terrestrial ecosystems and the atmosphere. *Journal of Agricultural Meteorology*, **2021**, 77(1), pp. 66-80.
13. Filella, I.; Primante, C.; Llusia, J.; Martin-Gonzalez, A.M.; Seco, R.; Farré-Armengol, G.; Rodrigo, A.; Bosch, J.; Penuelas, J. Floral advertisement scent in a changing plant-pollinators market. *Scientific reports*, **2013,** 3(1), pp. 1-6.
14. Lun, X.; Lin, Y.; Chai, F.; Fan, C.; Li, H.; Liu, J. Reviews of emission of biogenic volatile organic compounds (BVOCs) in Asia. *Journal of Environmental Sciences*, **2020,** 95, pp. 266-277.
15. Saunier, A.; Ormeño, E.; Boissard, C.; Wortham, H.; Temime-Roussel, B.; Lecareux, C.; Armengaud, A.; Fernandez, C. Effect of mid-term drought on Quercus pubescens BVOCs' emission seasonality and their dependency on light and/or temperature. *Atmospheric Chemistry and Physics*, **2017**, 17(12), pp. 7555-7566.
16. Caser, M.; Chitarra, W.; D'Angiolillo, F.; Perrone, I.; Demasi, S.; Lovisolo, C.; Pistelli, L.; Pistelli, L.; Scariot, V. Drought stress adaptation modulates plant secondary metabolite production in Salvia dolomitica Codd. *Industrial crops and products*, **2019,** 129, pp. 85-96.
17. Jiang, X.; Guenther, A.; Potosnak, M.; Geron, C.; Seco, R.; Karl, T.; Kim, S.; Gu, L.; Pallardy, S. Isoprene emission response to drought and the impact on global atmospheric chemistry. *Atmospheric Environment*, **2018**, 183, pp. 69-83.
18. Wang, H.; Wu, Q.; Guenther, A.B.; Yang, X.; Wang, L.; Xiao, T.; Li, J.; Feng, J.; Xu, Q.; Cheng, H. A long-term estimation of biogenic volatile organic compound (BVOC) emission in China from 2001–2016: the roles of land cover change and climate variability. *Atmospheric Chemistry and Physics*, **2021**, 21(6), pp. 4825-4848.
19. Meeningen, Y.V.; Schurgers, G.; Rinnan, R.; Holst, T. Isoprenoid emission response to changing light conditions of English oak, European beech and Norway spruce. *Biogeosciences*, **2017,** 14(18), pp. 4045-4060.
20. Medori, M.; Michelini, L.; Nogues, I.; Loreto, F.; Calfapietra, C. The impact of root temperature on photosynthesis and isoprene emission in three different plant species. *The Scientific World Journal*, **2012**, *.pp.* 525827
21. Alves, E.G.; Harley, P.; Gonçalves, J.F.D.C.; Moura, C.E.D.S.; Jardine, K. Effects of light and temperature on isoprene emission at different leaf developmental stages of Eschweilera coriacea in central Amazon. *Acta Amazonica*, **2014**, 44(1), pp. 9-18.
22. Melillo, J.M.; Richmond, T.T.; Yohe, G. Climate change impacts in the United States. Third national climate assessment. United State. 2014, pp.52.

23. Von Schneidemesser, E.; Monks, P.S.; Allan, J.D.; Bruhwiler, L.; Forster, P.; Fowler, D.; Lauer A.; Morgan W.T.; Paasonen, P.; Righi, M.; Sindelarova, K. Chemistry and the linkages between air quality and climate change. *Chemical Reviews*, **2015,** 115(10), pp. 3856-3897.
24. Sharkey, T.D.; Monson, R.K. The future of isoprene emission from leaves, canopies and landscapes. *Plant, Cell & Environment*, **2014,** 37(8), pp. 1727-1740.
25. Rosenkranz, M.; Pugh, T.A.; Schnitzler, J.P.; Arneth, A. Effect of land-use change and management on biogenic volatile organic compound emissions–selecting climate-smart cultivars. *Plant, cell & environment*, **2015,** 38(9), pp. 1896-1912.
26. Paasonen, P.; Asmi, A.; Petäjä, T.; Kajos, M.K.; Äijälä, M.; Junninen, H.; Holst, T.; Abbatt, J.P.; Arneth, A.; Birmili, W.; Van Der Gon, H.D.; Kulmala, M. Warming-induced increase in aerosol number concentration likely to moderate climate change. *Nature Geoscience*, **2013,** 6(6), pp. 438-442.
27. Carslaw, K.S.; Boucher, O.; Spracklen, D.V.; Mann, G.W.; Rae, J.G.L.; Woodward, S.; Kulmala, M. A review of natural aerosol interactions and feedbacks within the Earth system. *Atmospheric Chemistry and Physics*, **2013,** 10(4), pp. 1701-1737
28. Greenberg, J.P.; Asensio, D.; Turnipseed, A.; Guenther, A.B.; Karl, T.; Gochis, D. Contribution of leaf and needle litter to whole ecosystem BVOC fluxes. *Atmospheric Environment*, **2012,** 59, pp. 302-311.
29. Chen, W.H.; Guenther, A.B.; Wang, X.M.; Chen, Y.H.; Gu, D.S.; Chang, M.; Zhou, S.Z.; Wu, L.L.; Zhang, Y.Q. Regional to global biogenic isoprene emission responses to changes in vegetation from 2000 to 2015. *Journal of Geophysical Research: Atmospheres*, **2018,** 123(7), pp. 3757-3771.
30. Aydin, Y.M.; Yaman, B.; Koca, H.; Dasdemir, O.; Kara, M.; Altiok, H.; Dumanoglu, Y.; Bayram, A.; Tolunay, D.; Odabasi, M.; Elbir, T. Biogenic volatile organic compound (BVOC) emissions from forested areas in Turkey: Determination of specific emission rates for thirty-one tree species. *Science of the Total Environment*, **2014,** 490, pp. 239-253.
31. Liu, Y.; Li, L.; An, J.; Huang, L.; Yan, R.; Huang, C.; Wang, H.; Wang, Q.; Wang, M.; Zhang, W. Estimation of biogenic VOC emissions and its impact on ozone formation over the Yangtze River Delta region, China. *Atmospheric Environment*, **2018,** 186, pp. 113-128.
32. Wu, K.; Yang, X.; Chen, D.; Gu, S.; Lu, Y.; Jiang, Q.; Wang, K.; Ou, Y.; Qian, Y.; Shao, P.; Lu, S. Estimation of biogenic VOC emission and their corresponding impact on ozone and secondary organic aerosol formation in China. *Atmospheric Research*, **2020,** 231, pp. 104656.
33. Katragkou, E.; Zanis, P.; Kioutsioukis, I.; Tegoulias, D.; Melas, B.C.; Krüger, B.C.; Coppola, E. Future climate changes impact on summer surface ozone from regional climate-air-quality simulation over Europe. *Journal of Geophysical Research: Atmosphere*, **2011,** 116, pp. D22.
34. Bauwens, M.; Stavrakou, T.; Müller, J.F.; Van Schaeybroeck, B.; De Cruz, L.; De Troch, R.; Giot, O.; Hamdi, R.; Termonia, P.; Laffineur, Q.; Amelynck, C. Recent past (1979–2014) and future (2070–2099) isoprene fluxes over Europe simulated with the MEGAN–MOHYCAN model. *Biogeosciences*, **2018,** 15(12), pp. 3673-3690.
35. Nguyen, G.T.H.; Shimadera, H.; Uranishi, K.; Matsuo, T.; Kondo, A.; Thepanondh, S. Numerical assessment of PM2. 5 and O3 air quality in continental Southeast Asia: Baseline simulation and aerosol direct effects investigation. *Atmospheric Environment*, **2019,** 219, pp.117054.
36. Rahman, S.R.A.; Ismail, S.N.S.; Ramli, M.F.; Latif, M.T.; Abidin, E.Z.; Praveena, S.M. The assessment of ambient air pollution trend in Klang Valley, Malaysia. *World Environment*, **2015,** 5(1), pp. 1-11.
37. Robertson, A.W.; Moron, V.; Qian, J. H.; Chang, C.P.; Tangang, F.; Aldrian, E.; Koh, T.Y.; Liew, J. The maritime continent monsoon. In: The global monsoon system: research and forecast. World scientific publishing Co, Singapore, 2011; pp. 85-98.
38. Dong, Z.; Wang, L.; Sun, Y.; Hu, T.; Limsakul, A.; Singhruck, P.; Pimonsree, S. Heatwaves in Southeast Asia and their changes in a warmer world. *Earth's Future*, **2021,** 9(7), pp. e2021EF001992.
39. Arneth, A.; Schurgers, G.; Lathiere, J.; Duhl, T.; Beerling, D.J.; Hewitt, C.N.; Martin, M.; Guenther, A. Global terrestrial isoprene emission models: sensitivity to variability in climate and vegetation. *Atmospheric Chemistry and Physics*, **2011,** 11(15), pp. 8037-8052.
40. Sentian, J.; Payus, C.M.; Herman, F.; Kong, V.W.Y. Climate change scenarios over Southeast Asia. *APN Science Bulletin*, **2022,** 12, pp. 103-123.
41. Hurrell, J.W.; Holland, M.M.; Gent, P.R.; Ghan, S.; Kay, J.E.; Kushner, P.J.; Lamarque, J.F.; Large, W.G.; Lawrence, D.M.; Lindsay, K.; Lipscomb, W.H.; Long, M.C.; Mahowald, N.; Marsh, D.R.; Neale, R.B., Rasch, P.; Vavrus, S.; Vertenstein, M..; Bader, D.; Collins, W.D.; Hack, J.J.; Kiehl, J.T.; Marshall, S. The Community Earth System Model: A framework for collaborative research. *Bulletin of the American Meteorological Society*, **2013,** 94, pp. 1339-1360.
42. Taylor, K.E.; Stouffer, R.J.; Meehl, G. A. An overview of CMIP5 and the experiment design bull. *American Meteorological Society*, **2012,** 93, pp. 485-498.
43. IPCC. Climate change 2013: The physical science basis. Contribution of Working Group I to the Fifth Assessment Report of the Intergovernmental Panel on Climate Change. Cambridge University Press, Cambridge, UK and New York, NY. 2013.
44. Knutti, R.; Masson, D.; Gettelman, A. Climate model genealogy: Generation CMIP5 and how we got there. *Geophysical Research Letter*, **2013,** 40, pp. 1194-1199.
45. Thomson, A.M.; Calvin, K.V.; Smith, S.J.; Kyle, G.P.; Volke, A.; Patel, P.; Delgado-Arias, S.; Bond-Lamberty, B.; Wise, M.A.; Clarke, L.E.; Edmond, J.A. RCP4.5: A pathway for stabilization of radiative forcing by 2100. *Climate Change*, **2011,** 109, pp. 77-94.
46. Hijioka, Y.; Matsuoka, Y.; Nishimoto, H..; Masui, M.; Kainuma, M. Global GHG emissions scenarios under GHG concentration stabilization targets. *Journal of Global Environmental Engineering*, **2008,** 13, pp. 97-108.

47. Riahi, K.; Rao, S.; Krey, V.; Cho, C.; Chirkov, V.; Fischer, G.; kindermann, G.; Nakicenovic, N. RCP8.5 – A scenario of comparatively high greenhouse gas emissions. *Climatic Change*, **2011,** 109, pp. 33-57.
48. Guenther, A.; Karl, T.; Harley, P.; Wiedinmyer, C.; Palmer, P.I.; Geron, C. Estimates of global terrestrial isoprene emission using MEGAN (model of emissions of gases and aerosols from nature. *Atmospheric Chemistry and Physics*, **2006,** 6(11), pp. 3181-3210.
49. Guenther, A.B.; Zimmerman, P.R.; Harley, P.C.; Monson, R.K.; Fall, R. Isoprene and monoterpene emission rate variability – model evaluations and sensitivity analyses. *Journal of Geophysical Research: Atmospheres*, **1993,** 98, pp. 12609-12617.
50. Petron, G.; Harley, P.; Greenberg, J.; Guenther, A. Seasonal temperature variations influence isoprene emission. *Geophysical Research Letters*, **2001,** 28(9), pp. 1707-1710.
51. Sharkey, T.D.; Chen, X.; Yeh, S. Isoprene increases thermotolerance of fosmidomycin-fed leaves. *Plant physiology*, **2001,** 125(4), pp. 2001-2006.
52. Yuan, H.; Dai, Y.; Xiao, Z.; Ji, D.; Shangguan, W. Reprocessing the MODIS Leaf Area Index products for land surface and climate modelling. *Remote Sensing of Environment*, **2011,** 115(5), pp. 1171-1187.
53. Li, L.; Yang, W.; Xie, S.; Wu, Y. Estimations and uncertainty of biogenic volatile organic compound emission inventory in China for 2008–2018. *Science of The Total Environment*, **2020,** 733, pp. 139301.
54. Feng, Z.; Yuan, X.; Fares, S.; Loreto, F.; Li, P.; Hoshika, Y.; Paoletti, E. Isoprene is more affected by climate drivers than monoterpenes: A meta-analytic review on plant isoprenoid emissions. *Plant, cell & environment*, **2019,** 42(6), pp. 1939-1949.
55. Werner, C.; Fasbender, L.; Romek, K.M.; Yáñez-Serrano, A.M.; Kreuzwieser, J. Heat waves change plant carbon allocation among primary and secondary metabolism altering CO2 assimilation, respiration, and VOC emissions. *Frontiers in Plant Science*, **2020,** 11, pp**.** 1242
56. Kivimaenpaa, M.; Ghimire, R.P.; Sutinen, S.; Haikio, E.; Kasurinen, A.; Holopainen, T.; Holopainen J. K. Increase in volatile organic compound emission of scots pine in response to elevated ozone and warming are modified by herbivory and soil nitrogen availability. *Journal of Forest Research*, **2016,** 135, pp. 343-360.
57. Bamberger, I.; Ruehr, N.K.; Schmitt, M.; Gast, A.; Wohlfahrt, G.; Arneth, A. Isoprene emission and photosynthesis during heatwaves and drought in black locus. *Biogeosciences*, **2017,** 14(15), pp. 3649-3667.
58. Guidolotti, G.; Pallozzi, E.; Gavrichkova, O.; Scartazza, A.; Mattioni, M..; Loretto, F.; Calfapietra, C. Emission of constitutive isoprene, induced monoterpenes and other volatiles under high temperature in, eucalyptus camaldulensis, a 13C labelling study. *Plant, Cell & Environment*, **2019,** 42(6), pp. 1929-1938.
59. Lin, W.; Zhao, Z.; Lai, J.M.; Liu, Y.F.; Huang, X.R.; Yi, Z.G. Effects of temperature and light on isoprene and monoterpene emission from Loropetalum chinense and Nandina domestica. *Acta Scientiae Circumstantiae*, **2019,** 39, pp. 3126-3133
60. Chen, W.H.; Guenther, A.B.; Wang, X.M.; Chen, Y.H.; Gu, D.S.; Chang, M.; Zhou, S.Z.; Wu, L.L.; Zhang, Y.Q. Regional to global biogenic isoprene emission responses to changes in vegetation from 2000 to 2015. *Journal of Geophysical Research: Atmospheres*, **2018,** 123(7), pp. 3757-3771.
61. Supharatid, S.; Nafung, J.; Aribarg, T. Projected changes in temperature and precipitation over mainland Southeast Asia by CMIP6 models. *Journal of Water and Climate Change*, **2022,** 13(1), pp. 337-356.
62. Almazroui, M.; Saeed, S.; Saeed, F.; Islam, M.N.; Ismail, M. Projections of precipitation and temperature over the South Asian Countries in CMIP6. *Earth System and Environment*, **2020,** 4, pp. 297-320.
63. Thirumalai, K; DiNezio, P.N.; Okumura, Y.; Deser, C. Extreme temperatures in Southeast Asia caused by El Nino and worsened by global warming. *Nature communication*, **2017,** 8, pp. 15531.
64. Raghavan, S.V.; Hur, J.; Liong, S.Y. Evaluations of NASA NEX-GDDP data over Southeast Asia: present and future climates. *Climatic Change*, **2018,** 148, pp. 503-518.
65. Gasparrini A; Guo, Y,; Sera, F,; Vicedo-Cabrera, A.M..; Huber, V.; Tong, S.; de Sousa-Zanotti Stagliorio-Coelho, M.; Nascimento Saldiva, P.H.; Lavigne, E.; Matus-Correa, P.; Valdes-Ortega, N, Kan, H.; Osorio, S.; Kyselý, J.; Urban, A.; Jaakkola, J.J.K.; Ryti, N.R.I.; Pascal, M.; Goodman, P.G.; Zeka, A.; Michelozzi, P.; Scortichini, M.; Hashizume, M.; Honda, Y.; Hurtado-Diaz, M.; Cesar Cruz, J.; Seposo, X.; Kim, H.; Tobias, A.; Iñiguez, C.; Forsberg, B.; Åström, D.O.; Ragettli, M.S., Guo, Y.L.; Wu, C.F.; Zanobetti, A.; Schwartz, J.; Bell, M.L.; Dang, T.N.; Van, D.D.; Heaviside, C.; Vardoulakis, S.; Hajat, S.; Haines, A.; Armstrong, B. Projections of temperature-related excess mortality under climate change scenarios. *Lancet Planet Health*. **2017**, Dec;1(9), pp. 360-367.
66. Sentian, J.; MacKenzie, R.A.; Hewitt, C.N. The Regional Biogenic Emissions Response to Climate Changes and Ambient CO 2 in Southeast Asia. *International Journal of Climate Change*: *Impacts & Responses*, **2011,** 2(3), pp. 125-142.
67. Kong, S.S.K.; Sentian, J.; Bidin, K. Future simulation of solar radiation and cloud fraction over the Malaysia Region under RCP 4.5 and RCP 8.5 scenarios. *Journal of Engineering and Applied Sciences*. **2017,** 12(12), pp. 3042-3050.
68. Uning, R.; Latif, M.T.; Othman, M..; Juneng, L.; Mohd Hanif, N.; Nadzir, M.S.M..; Abdul Maulud, K.N.; Jaafar, W.S.W.M.; Said, N.F.S.; Ahamad, F.; Takriff, M.S. A review of Southeast Asian oil palm and Its CO2 fluxes. *Sustainability*, **2020,** 12(12), pp. 5077.
69. Hewitt, C.N.; MacKenzie, A.R..; Di Carlo, P.; Di Marco, C.F.; Dorsey, J.R.; Evans, M.; Fowler, D.; Gallagher, M.W.; Hopkins, J.R.; Jones, C.E.; Langford, B.; Stewart, D.J. Nitrogen management is essential to prevent tropical oil palm plantations from causing ground-level ozone pollution. *Proceedings of the National Academy of Sciences*, **2009,** 106(44), pp. 18447-18451.
70. Oku, H.; Inafuku, M.; Takamine, T.; Nagamine, M.; Saitoh, S.; Fukuta, M. Temperature threshold of isoprene emission from tropical trees, Ficus virgata and Ficus septica. *Chemosphere*, **2014,** 95, pp. 268-273.
71. Mutanda, I.; Inafuku, M.; Saitoh, S.; Iwasaki, H.; Fukuta, M.; Watanabe, K.; Oku, H. Temperature controls on the basal emission rate of isoprene in a tropical tree Ficus septica: exploring molecular regulatory mechanisms. *Plant, cell & environment*, **2016,** 39(10), pp. 2260-2275.

72. Arneth, A.; Niinemets, Ü.; Pressley, S.; Bäck, J.; Hari, P.; Karl, T.; Noe, S.; Prentice, I.C.; Serça, D.; Hickler, T.; Wolf, A. Process-based estimates of terrestrial ecosystem isoprene emissions: incorporating the effects of a direct CO2-isoprene interaction. *Atmospheric Chemistry and Physics*, **2007,** 7(1), pp. 31-53.
73. Schurgers, G.; Mikolajewicz, U.; Gröger, M..; Maier-Reimer, E.; Vizcaíno, M.; Winguth, A. The effect of land surface changes on Eemian climate. *Climate dynamics*, **2007,** 29(4), pp. 357-373.
74. Heald, C.L.; Wilkinson, M.J.; Monson, R.K.; Alo, C.A.; Wang, G.; Guenther, A. Response of isoprene emission to ambient CO2 changes and implications for global budgets. *Global Change Biology*, **2009,** 15(5), pp. 1127-1140.
75. Tai, A.P.K.; Mickley, L.J.; Heald, C.L.; Wu, S. Effect of CO inhibition on biogenic isoprene emission: Implication for air quality under 2000 to 2050 changes in climate, vegetation, and land use. *Geophysical Research Letter*, **2013,** 40, pp.3479-3483.
76. Tang, J.; Schurgers, G.; Valolahti, H.; Faubert, P.; Tiiva, P.; Michelsen, A.; Rinnan, R. Challenges in modelling isoprene and monoterpene emission dynamics of Arctic plants: a case study from a subarctic tundra heath. *Biogeosciences*, **2016,** 13(24), pp. 6651-6667.
77. De Swaef, T.; Steppe, K. Linking stem diameter variations to sap flow, turgor and water potential in tomato. *Functional Plant Biology*, **2010,** 37(5), pp. 429-438.
78. Zhou, T.; Yu, R.; Zhang, J.; Drange, H..; Cassou, C.; Deser, C.; Hodson, D.L.R..; Sanchez-Gomez, E.; Li, J.; Keenlyside, X.; Okumura, Y. Why the western Pacific subtropical high has extended westward since the late 1970s. *Journal of Climate*, **2014,** 22(8), pp. 2199-2215.
79. Huang, J.; Hartmann, H.; Hellén, H.; Wisthaler, A.; Perreca, E.; Weinhold, A.; Rücker, A.; van Dam, N.M.; Gershenzon, J.; Trumbore, S.; Behrendt, T. New perspectives on CO2, temperature, and light effects on BVOC emissions using online measurements by PTR-MS and cavity ring-down spectroscopy. *Environmental science & technology*, **2018,** 52(23), pp. 13811-13823.
80. Baker, B.; Bai, J.H..; Johnson, C.; Cai, Z.T.; Li, Q.J.; Wang, Y.F.; Guenther, A.; Greenberg, J.; Klinger, L.; Geron, C.; Rasmussen, R. Wet and dry season ecosystem level fluxes of isoprene and monoterpenes from a southeast Asian secondary forest and rubber tree plantation. *Atmospheric Environment*, **2005,** 39(2), pp. 381-390.
81. Brilli, F.; Barta, C.; Fortunati, A.; Lerdau, M.; Loreto, F.; Centritto, M. Response of isoprene emission and carbon metabolism to drought in white poplar (Populus alba) saplings. *New Phytologist*, **2007,** 175(2), pp. 244-254.
82. Harrison, S.P.; Morfopoulos, C.; Dani, K.S.; Prentice, I.C.; Arneth, A.; Atwell, B.J.; Barkley, M.P.; Leishman, M.R.; Loreto, F.; Medlyn, B.E.; Niinemets, Ü. Volatile isoprenoid emissions from plastid to planet. *New Phytologist*, **2013,** 197(1), pp. 49-57.
83. Li, L.Y.; Xie, S.D. Historical variations of biogenic volatile organic compound emission inventories in China, 1981–2003. *Atmospheric environment*, **2014,** 95, pp. 185-196.
84. Hantson, S.; Knorr, W.; Schurgers, G.; Pugh, T.A.; Arneth, A. Global isoprene and monoterpene emissions under changing climate, vegetation, CO2, and land use. *Atmospheric Environment*, **2017,** 155, pp. 35-45.
85. Mu, Z.; Llusià, J.; Zeng, J.; Zhang, Y.; Asensio, D.; Yang, K..; Yi, Z.; Wang, X.; Peñuelas, J. An Overview of the Isoprenoid Emissions From Tropical Plant Species. *Frontiers in Plant Science*, **2022,** 13, pp. 833030.
86. Loo, Y.Y.; Billa, L.; Singh, A. Effect of climate change on seasonal monsoon in Asia and its impact on the variability of monsoon rainfall in Southeast Asia. *Geoscience Frontiers*, **2015,** 6(6), pp. 817-823.